REPORT DOCUMENTATION PAGE

The public reporting burden for this collection of information is estimated to average 1 hour per response, including the time for r
gathering and maintaining the data needed, and completing and reviewing the collection of information. Send comments regarding th
of information, including suggestions for reducing the burden, to Department of Defense, Washington Headquarters Services
(0704-0188), 1215 Jefferson Davis Highway, Suite 1204, Arlington, VA 22202-4302. Respondents should be aware that notwithstanding any other provision of law, no person shall be
subject to any penalty for failing to comply with a collection of information if it does not display a currently valid OMB control number.
PLEASE DO NOT RETURN YOUR FORM TO THE ABOVE ADDRESS.

1. REPORT DATE *(DD-MM-YYYY)* 29062004	2. REPORT TYPE Final Report	3. DATES COVERED *(From - To)* 1 Aug 2003 - 31 Dec 2003

4. TITLE AND SUBTITLE Fundamental Studies of Liquid-Propellant Rocket Combustion	5a. CONTRACT NUMBER
	5b. GRANT NUMBER F49620-03-1-0378
	5c. PROGRAM ELEMENT NUMBER
6. AUTHOR(S) Forman A. Williams	5d. PROJECT NUMBER
	5e. TASK NUMBER
	5f. WORK UNIT NUMBER

7. PERFORMING ORGANIZATION NAME(S) AND ADDRESS(ES) Department of Mechanical and Aerospace Engineering University of California, San Diego LaJolla CA 92093-0411

20040810 015

9. SPONSORING/MONITORING AGENCY NAME(S) AND ADDRESS(ES) USAF/AFRL AFOSR 801 N. Randolph Street Arlington VA 22203	AFOSR
	11. SPONSOR/MONITOR'S REPORT NUMBER(S)

12. DISTRIBUTION/AVAILABILITY STATEMENT

Distribution Statement A. Approved for public release; distribution is unlimited.

13. SUPPLEMENTARY NOTES

14. ABSTRACT
This research was directed towards developing new knowledge of combustion processes in liquid-propellant rocket engines. Attention was given to the combustion of different fuels, beginning with hydrogenoxygen but ultimately including multicomponent hydrocarbon mixtures representative of RP fuels, and to nonlinear processes of importance in combustion instability. Effects of detailed chemical kinetics on performance and stability were addressed by introducing systematically reduced chemistry that enables theoretical analyses to be completed thoroughly and accurately. The interactions between chemistry and turbulence were addressed, including the effects of the heat release on the turbulance. The orientation of the work was fundamental and aimed at predicting not only performance and acoustic response but also intrinsic instability. The results were intended to help to improve understanding of combustion mechanisms and combustion instabilities in liquid-propellant rocket motors. The most recent specific results concern induction times in hydrogen-oxygen mixtures and heal-release effects on turbulent mixiing.

15. SUBJECT TERMS

16. SECURITY CLASSIFICATION OF:			17. LIMITATION OF ABSTRACT	18. NUMBER OF PAGES	19a. NAME OF RESPONSIBLE PERSON
a. REPORT	b. ABSTRACT	c. THIS PAGE			
U	U	U	UU	5	19b. TELEPHONE NUMBER *(Include area code)*

Standard Form 298 (Rev. 8/98)
Prescribed by ANSI Std. Z39.18

8-4-04

Fundamental Studies of Liquid-Propellant Rocket Combustion

Forman A. Williams
Department of Mechanical and Aerospace Engineering
University of California, San Diego
La Jolla, CA 92093-0411
Tel: (858) 534-5492; Fax: (858) 534-5354; Email: faw@ucsd.edu

Final Technical Report, June 29, 2004

Abstract

This research was directed towards developing new knowledge of combustion processes in liquid-propellant rocket engines. Attention was given to the combustion of different fuels, beginning with hydrogen-oxygen but ultimately including multicomponent hydrocarbon mixtures representative of RP fuels, and to nonlinear processes of importance in combustion instability. Effects of detailed chemical kinetics on performance and stability were addressed by introducing systematically reduced chemistry that enables theoretical analyses to be completed thoroughly and accurately. The interactions between chemistry and turbulence were addressed, including the effects of the heat release on the turbulence. The orientation of the work was fundamental and aimed at predicting not only performance and acoustic response but also intrinsic instability. The results were intended to help to improve understanding of combustion mechanisms and combustion instabilities in liquid-propellant rocket motors. The most recent specific results concern induction times in hydrogen-oxygen mixtures and heal-release effects on turbulent mixing.

Research Highlights

Above the second explosion limit, the ignition of hydrogen mixtures is known to exhibit a relatively long period of chain-carrier growth prior to significant heat release, which occurs through chain recombination once a sufficiently large radical pool has formed. Since this induction period typically represents a considerable fraction of the overall combustion time, designs of hydrogen combustion devices must account for this delay. Because of its practical importance, the induction time in hydrogen-air ignition has remained an active research topic for over 40 years. Numerous shock-tube experimental measurements of hydrogen induction times are available [1]-[9]. The criteria used in experiments for defining the induction time vary. Thus, for some authors the induction period ends at the onset of luminosity or as the pressure rises above a given threshold value as a result of heat release, while others prefer to relate the induction time, t_i, to the radical concentration through OH emission or absorption. Under most conditions, in contrast to ignition of many other fuels, the resulting value of t_i for hydrogen depends only weakly on the definition used.

In addition to the experimental work, there have been a number of analytical studies devoted to the calculation of the hydrogen-oxygen induction time at high temperature [1, 5, 6, 7, 10, 11]. Although the success of many of these previous analytical and computational efforts has been limited by uncertainties in reaction-rate kinetics, these works provided much understanding on the induction process. For instance, Schott and Kinsey [1] already anticipated that the radicals O and OH follow a steady-state approximation if the mixture is sufficiently rich, a result that Treviño [11] obtained later in his systematic reduction of the ignition chemistry. The induction time was determined in [1] from the evolution of the H-atom concentration, the only species out of steady state. Both reactant consumption and heat release were seen to be negligible during this initial stage of radical growth, giving an H-atom concentration that increases exponentially in time. Since $H + O_2 \rightarrow OH + O$ is the rate-limiting reaction, the resulting induction time was seen to be proportional to the reciprocal of the initial oxygen concentration [1]. The calculation procedure can be extended by accounting for a larger number of radicals, as done in [5, 6, 7, 10], to give a system of linear differential equations for the radical-pool evolution. The resulting induction time becomes inversely proportional to the largest eigenvalue of the associated eigenvalue problem, showing a dependence on the mixture composition more complex than that of rich mixtures.

The present work combines the knowledge currently available on the H_2-O_2 kinetics [12]-[15] with the procedure outlined above for the calculation of t_i [5, 6, 7, 10], thereby providing an improved theoretical

prediction for the induction time, valid under variable conditions of pressure, temperature and composition. The kinetics of hydrogen combustion is now well established, and only small differences (mainly in reaction-rate constants) exist between the different mechanisms currently available (e.g., [12]-[15]). Use of these chemical-kinetic mechanisms enable the calculation of ignition histories by numerical integration of the conservation equations for species and energy in a homogeneous mixture at constant pressure. Results of such detailed-chemistry computations are compared in Fig. 1 with the experimental measurements of Just and Schmalz [7] and Bhaskaran et al. [8], the induction time being identified in the numerical computations with the peak H-atom concentration. The results obtained with the different mechanisms are very similar; significant discrepancies are only found as the crossover temperature of the second explosion limit [16] is approached. From the comparisons with the experimental results, it can be inferred that the mechanism of Miller and Bowman [13] tends to underpredict the crossover temperature, while the GRI mechanism [14] and that compiled by Maas and Warnatz [12] tend to overpredict it. For the four conditions of pressure and composition used in the figure, the San Diego mechanism [15], developed in the present project, is the one that shows the best agreement with the experiments over the whole range of temperatures considered. In view of these results, the analytical development uses the reaction rates given in internet-based updated version of [15].

The reaction mechanisms [12]-[15] comprise about 20 reversible reactions among 8 reactive species, including as intermediates H, O, OH, HO_2 and H_2O_2. The numerical computations indicate that the six steps suffice to describe accurately the induction period. The rate constants vary with the temperature T according to $k_i = A_i T^{n_i} \exp(-T_{a_i}/T)$ [15], where the units are mol/cm^3, s^{-1} and K. Nonunity chaperon efficiencies of 0.3 for O_2 and 7.0 for H_2O must be considered when calculating the third-body concentration c_M appearing in the rate of reaction 5 [15]. Note that the present short mechanism does not consider HO_2 consumption, a simplification that may introduce small inaccuracies in induction times very close to crossover [4].

No.	Reactions	A	n	T_a
0	$H_2 + O_2 \rightarrow OH + OH$	1.70×10^{13}	0.0	24044
1	$H_2 + O_2 \rightarrow HO_2 + H$	2.91×10^{12}	0.47	26800
2	$H + O_2 \rightarrow OH + O$	3.52×10^{16}	-0.7	8535
3	$O + H_2 \rightarrow OH + H$	5.06×10^{4}	2.7	3145
4	$OH + H_2 \rightarrow H_2O + H$	1.17×10^{9}	1.3	1813
5	$H + O_2 + M \rightarrow HO_2 + M$	2.6×10^{19}	-1.2	0

As can be seen, two different initiation reactions are considered in the mechanism, while others that are much slower, such as $H_2 \rightarrow 2H$, are neglected. Except for an early investigation [10], all previous efforts have used only one of the two reactions, i.e., reaction 0 is selected in [1, 5, 6] while reaction 1 is preferred in [7, 11]. The rate constant for $H_2 + O_2 \rightarrow OH + OH$ was first estimated by Semenov [17] and later improved by Ripley and Gardiner [18]. The reaction-rate parameters given above for 0 are those proposed by Jachimowski and Houghton [19], which are adopted by the four currently used mechanisms [12]-[15]. The rate of reaction 1 is determined from measurements of the inverse reaction $HO_2 + H \rightarrow H_2 + O_2$. Experimental data collected in the eighties [20, 21, 22] have been used to determine the reaction-rate parameters used for this reaction in [12]-[15]. The different constants k_1 differ only moderately over the range of temperatures of interest (1000 K < T < 4000 K), e.g., by less than ten percent for the two internet-based mechanisms [14, 15]. With the rate constants proposed in [15] reaction 1 is the dominant chain-initiation reaction at temperatures below T $\simeq$ 2315 K, and the opposite behavior is observed above this temperature. Therefore, both reactions must in principle be retained in the mechanism for increased accuracy.

The analytical development addresses three differential equations for the time development, which can be written nondimensionally as

$$dy_H/d\tau = -(\varepsilon + 1/2)y_H + y_O + y_{OH} + \nu_0, \tag{1}$$

$$dy_O/d\tau = (\phi/\kappa_O)(y_H/2 - y_O) \tag{2}$$

and

$$dy_{OH}/d\tau = (\phi/\kappa_{OH})(y_H/2 + y_O - y_{OH} + \nu_1). \tag{3}$$

The asymptotic analysis results in explicit simple formulas for the induction times for large and small values of the equivalence ratio ϕ and a more complex exact solution that applies for all ϕ. Figure 2 compares these results. It is seen that the asymptotic result for lean mixtures, which has H in steady state, is good for $\phi \leq 0.07$, the asymptotic result for stoichiometric and rich mixtures, which has O and OH in steady state, is good for $\phi \geq 1$, and in the intermediate range $0.07 \leq \phi \leq 1$ all three radicals are out of steady state, and the more complex exact solution is needed. Nevertheless, the sum of the two asymptotic results provides induction times that are correct within and order of magnitude over the entire range of equivalence ratio.

In other recent work, evaluations were made of DNS (direct numerical simulation) results for the mixture-fraction scalar Z and the scalar dissipation χ in temporally evolving shear layers. Effects of high heat release have not been available previously. For high heat release, typical of hydrocarbon combustion, the mixing was found to be substantially different than without heat release. The probability-density function of the scalar and the conditional rate of scalar dissipation were found to be affected by the heat release in such a way that the heat release substantially decreases the overall reaction rate. To help clarify implications of the assumptions underlying popular models for interaction between turbulence and chemistry, the local structure of the scalar dissipation rate at the reaction sheet was extracted from the DNS database. The applicability of flamelet models for the rate of scalar dissipation was examined. To assist in modeling, a characteristic length scale was defined, representing the distance around the reaction sheet over which the scalar field is locally linear, and statistical properties of this length scale were investigated. This length scale can be used to investigate values of the rate of scalar dissipation that mark the boundary between flames that feel a constant scalar dissipation field and those that do not.

The topology of isoscalar surfaces is central to validity of assumptions underlying modeling of nonpremixed turbulent combustion. This is especially true for flamelet approaches that rely on expansions about the stoichiometric value $Z = Z_s$, but it also applies to other approaches that deal with averages of χ conditioned on Z. The simplest conceivable configuration is that of a planar stagnant molecular mixing layer, in which isoscalar surfaces are parallel planes, and $\sqrt{D/\chi}$ is constant everywhere, where D is the scalar diffusion coefficient. Since this uniformity of $|\nabla Z|$ from $Z = 0$ to $Z = 1$ is unrealistic in turbulence, steady counterflow laminar flamelet models have been considered, which maintain parallel planar isoscalar surfaces but have $|\nabla Z|$ varying smoothly from zero at $Z = 0$ or at $Z = 1$ to a maximum near $Z = 0.5$ in each instantaneous realization. Turbulence, however, generates much more complex topology than this for isoscalar surfaces, causing them to be nonplanar and time-dependent, a fact that is responsible for the known limitations of steady laminar flamelet models, including those that take into account the linear variation of χ with Z near $Z = Z_s$. Turbulence can generate more than mild wrinkles in the curves on space-time-resolved bases. Ridges can develop, with $|\nabla Z|$ achieving minima along certain surfaces, as well as zero-gradient points, where $\chi = 0$. The wrinkles readily produce maxima and minima in instantaneous plots of χ as a function of Z along paths in the direction of ∇Z, and the minima descend to $\chi = 0$ at zero-gradient points. Such plots must in fact end when $\chi = 0$, turning back on themselves in at least one other maximum-gradient direction, at maximum or minimum values of Z different from 1 or 0, unless the zero-gradient point has an inflection type of behavior instead of being a local absolute extremum. These complexities deserve consideration in modeling.

A first step in this direction is to study in greater detail the local behaviors of the Z and χ fields in the vicinity of isoscalar surfaces. Let y be the distance in the direction normal to the surface $Z = Z_s$, with $y > 0$ for $Z > Z_s$ and $y < 0$ for $Z < Z_s$. A Taylor expansion through second order in y then is

$$Z = Z_s + a_1 y + a_2 y^2, \tag{4}$$

where

$$a_1 = \sqrt{\left(\frac{\partial Z}{\partial x_i}\right)^2} \tag{5}$$

and

$$a_2 = \frac{1}{2} n_i n_j \frac{\partial^2 Z}{\partial x_i \partial x_j}, \tag{6}$$

in which
$$n_i = \frac{1}{a_1} \frac{\partial Z}{\partial x_i} \tag{7}$$

is the i'th component of a unit vector normal to the surface. All partial derivatives here are evaluated the point where $Z = Z_s$. The second coefficient, a_2, differs from the curvature of the isoscalar surface $Z = Z_s$ itself, which is

$$\frac{\partial n_i}{\partial x_i} = \frac{1}{a_1}\left(\frac{\partial^2 Z}{\partial x_i^2} - n_i n_j \frac{\partial^2 Z}{\partial x_i \partial x_j} \right). \tag{8}$$

Both a_1 and a_2 are random variables. Since $\chi = 2Da_1^2$, there have, in effect, been numerous statistical studies of a_1, but a_2 has been relatively neglected. The expansion of χ about $Z = Z_s$, however, depends on a_2. Through first order in $(Z - Z_s)$,

$$\chi = \chi_s + \frac{d\chi}{dZ}\bigg|_{Z=Z_s} (Z - Z_s), \tag{9}$$

where

$$\frac{d\chi}{dZ}\bigg|_{Z=Z_s} = 4D\frac{d^2Z}{dy^2} + 2\frac{dD}{dZ}\left(\frac{dZ}{dy}\right)^2 = 8Da_2 + 2\frac{dD}{dZ}a_1^2, \tag{10}$$

the last term of which may be neglected because D typically reaches a maximum very near $Z = Z_s$. The good approximation

$$a_2 = \frac{1}{8D_s}\frac{d\chi}{dZ}\bigg|_{Z=Z_s} \tag{11}$$

thus relates a_2 to the slope of the curve of χ as a function of Z at $Z = Z_s$. Since, according to this equation, stagnant mixing-layer flamelet models have $a_2 = 0$, while steady counterflow laminar flamelet models with $Z_s < 0.5$ have $a_2 > 0$, the statistics of a_2 pertains to the potential applicability of these models.

Another reason for interest in a_2 is its relevance to limitations on the use of the characteristic length

$$\ell = Z_s\sqrt{2D_s/\chi_s} = Z_s/a, \tag{12}$$

often considered in turbulence modeling. This length defines the characteristic distance over which Z varies by a fractional amount of order unity only when the quadratic term a_2 is small compared with the linear term. This condition breaks down when $|y|$ becomes of order

$$d = a_1/|a_2|. \tag{13}$$

The departure of Z from Z_s at this limit is

$$\Delta Z = Z_s d/\ell = a_1^2/|a_2|, \tag{14}$$

which may be called the limiting scalar deviation in that Z ceases to vary linearly with distance y beyond this deviation. It thus is a measure of the amplitude of wrinkles of curves of Z as a function of distance normal to isoscalar surfaces. This limiting deviation and the associated limiting length, d, which is the characteristic linear dimension or length of such wrinkles, are random variables having statistics determined by those of a_1 and a_2. The statistics of a_1 and a_2, conditional on $Z = Z_s$, thus have bearings on a number of questions.

Graphs of the conditional averages of χ as functions of Z were investigated in this work. These averages are basically equivalent to conditional averages of a_1. Corresponding graphs of conditional averages of a_2 also were investigated. For heat release $Q = 0$ they are antisymmetric about $Z = 0.5$, as they must be. They are also very nearly antisymmetric for $Q \neq 0$, suggesting that, although the dynamics correspond to $Z_s = 0.2$ in these cases, contrary to a_1 the asymmetry of the density field has little effect on the conditioned mean a_2, thereby allowing any value of Z to be interpreted as Z_s. The density change has little effect on the conditional mean $\langle a_2|Z \rangle$ for $0.3 \leq Z \leq 0.7$, but there are noticeable influences in the extremes representative of hydrocarbon combustion. The conditioned means all peak near $Z = 0.1$, but the peak for $Q = 0$ is much higher than those for $Q \neq 0$. The heat release of combustion therefore reduces a_2, which would tend to increase the limiting scalar deviation and the wrinkle length.
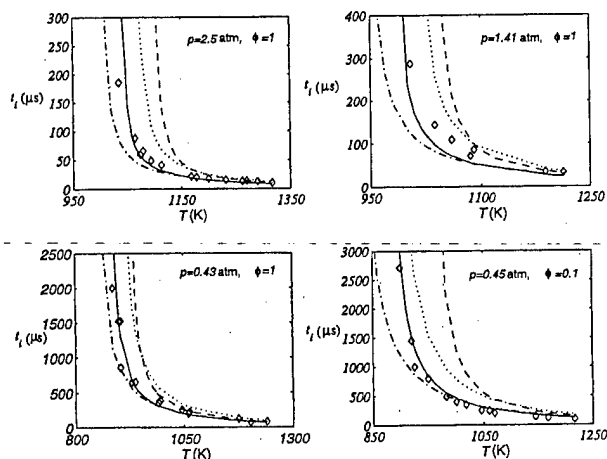
Figure 1: The lines represent the variation with temperature of the induction time as obtained from detailed-chemistry numerical computations (solid lines: SD mechanism [15], dotted lines: Maas and Warnatz [12], dashed lines: GRI [14], dot-dashed lines: Miller and Bowman [13]), while the symbols denote the shock-tube experimental results of Just and Schmalz [7] (p = 0.41, 0.43, 1.41 atm) and of Bhaskaran et al. [8] (p = 2.5 atm).
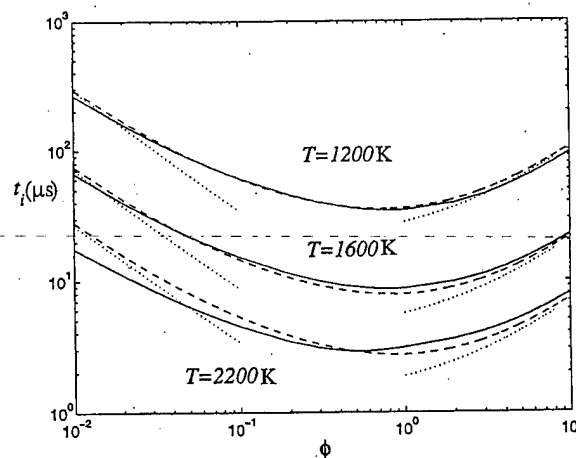
Figure 2: The induction time at atmospheric pressure as obtained from integrations of the full conservation equations (solid lines), from evaluations of the exact solution to (1)-(3) (dashed lines), and from evaluations of the asymptotic predictions (dotted lines).

Relevance / Transitions

- New high-performance rockets need liquid propellants for specific impulse, control and throttling.
- Codes predicting performance and instability can give wrong results because of wrong chemistry.
- Correct chemistry is too complicated for codes.
- Reduced chemistry retains essentials of correct chemistry but is simple enough to use in codes.
- Result is improved prediction of motor performance and instability.
- Recent applications have been to predicting emissions of oxides of nitrogen in turbulent combustors using KIVA code (Solar Turbines) and predicting autoignition of natural gas in dual-fuel diesel engines (BKM Co.).
- Rocket applications pertain to space launch, long-range missiles and high-altitude maneuverability.
- Propellant combinations include LOX-hydrogen and LOX-RP.
- Other major contributions have been:
  1. Discovery of bimodal probability-density function for combustion instability as a result of nonlinear subcritical bifurcation, explaining why liquid-propellant rockets can sometimes jump from stable burning to noisy high-amplitude acoustic instability.
  2. Explanation of Hewitt empirical correlation for stable and unstable LOX/RP-1 rockets with like-on-like injector, in a diagram of frequency and ratio of injector diameter to injection velocity, on the basis of acoustic amplification by mixing-layer combustion.
  3. Identification of cause of droplet burning time being minimum at critical pressure, on the basis of three-component phase diagrams, explaining new mechanism of combustion instability at near-critical conditions, with more stable operation at subcritical or supercritical conditions.
  4. Development of two-step to four-step reduced chemistry for hydrogen-oxygen and hydrocarbon-oxygen rocket combustion, providing accurate, fundamentally based and practically useable description for calculating liquid-propellant rocket performance and instability.

6/29/04